Temporal Relationship Between Visual Field, Retinal and Microvascular Pathology Following ^{125}I-Plaque Brachytherapy for Uveal Melanoma

Michelle R. Tamplin,[1] Wenxiang Deng,[2,3] Mona K. Garvin,[2,3] Elaine M. Binkley,[4] Daniel E. Hyer,[5] John M. Buatti,[5] Johannes Ledolter,[2,6] H. Culver Boldt,[4] Randy H. Kardon,[2,4] and Isabella M. Grumbach[1,2,7]

[1]Free Radical and Radiation Biology Program, Department of Radiation Oncology, University of Iowa, Iowa City, Iowa, United States
[2]Iowa City VA Center for the Prevention and Treatment of Visual Loss, Iowa City, Iowa, United States
[3]Department of Electrical and Computer Engineering, University of Iowa, Iowa City, Iowa, United States
[4]Department of Ophthalmology and Visual Sciences, University of Iowa, Iowa City, Iowa, United States
[5]Department of Radiation Oncology, University of Iowa, Iowa City, Iowa, United States
[6]Henry B. Tippie College of Business, University of Iowa, Iowa City, Iowa, United States
[7]Abboud Cardiovascular Research Center, Division of Cardiovascular Medicine, Department of Internal Medicine, Carver College of Medicine, University of Iowa, Iowa City, Iowa, United States

Correspondence: Isabella Grumbach, Division of Cardiovascular Medicine, Department of Internal Medicine, Carver College of Medicine, University of Iowa, Iowa City, IA, 52242, USA; isabella-grumbach@uiowa.edu.

Received: July 13, 2020
Accepted: December 4, 2020
Published: January 4, 2021

Citation: Tamplin MR, Deng W, Garvin MK, et al. Temporal relationship between visual field, retinal and microvascular pathology following ^{125}I-plaque brachytherapy for uveal melanoma. *Invest Ophthalmol Vis Sci.* 2021;62(1):3. https://doi.org/10.1167/iovs.62.1.3

Purpose. To define the temporal relationship of vascular versus neuronal abnormalities in radiation retinopathy.

Methods. Twenty-five patients with uveal melanoma treated with brachytherapy and sixteen controls were tested. Functional outcome measures included visual acuity and threshold perimetry (HVF 10-2), while structural outcomes included retinal thickness by OCT and vascular measures by OCT angiography and digital fundus photography. The degree of structural abnormality was determined by intereye asymmetry compared with normal subject asymmetry. Diagnostic sensitivity and specificity of each measure were determined using receiver operating characteristic curves. The relationships between the outcome measures were quantified by Spearman correlation. The effect of time from brachytherapy on visual function, retinal layer thickness, and capillary density was also determined.

Results. Within the first 2 years of brachytherapy, outcome measures revealed visual field loss and microvascular abnormalities in 38% and 31% of subjects, respectively. After 2 years, they became more prevalent, increasing to 67% and 67%, respectively, as did retinal thinning (50%). Visual field loss, loss of capillary density, and inner retinal thickness were highly correlated with one another. Diagnostic sensitivity and specificity were highest for abnormalities in digital fundus photography, visual field loss within the central 10°, and decrease in vessel density.

Conclusions. Using quantitative approaches, radiation microvasculopathy and visual field defects were detected earlier than loss of inner retinal structure after brachytherapy. Strong correlations eventually developed between vascular pathology, change in retinal thickness, neuronal dysfunction, and radiation dose. Radiation-induced ischemia seems to be a primary early manifestation of radiation retinopathy preceding visual loss.

Keywords: radiation retinopathy, microvasculopathy, uveal melanoma

^{125}I-Plaque brachytherapy is widely used to treat uveal melanoma, the most common form of primary intraocular cancer in adults.[1] With this therapy, local tumor control is achieved in 95% or more cases,[2,3] making it the preferred treatment for patients with medium-sized melanomas desiring globe-sparing therapy; however, at least 50% of patients will develop significant vision loss within 3 to 5 years of their radiation therapy.[4–7] Although a number of conditions (i.e., radiation-induced cataracts and keratopathy) contribute to morbidity after brachytherapy,[8,9] the long-term adverse effects have been attributed largely to damage of the retinal, choroidal, and optic nerve vasculature.[10] This finding is consistent with reports of extensive microvascular pathology, including capillary loss more than 24 months after therapy, as shown by the Collaborative Ocular Melanoma Study and other trials.[7,11] It has been postulated that the subclinical, acute radiation damage to the vascular endothelium precedes later stage, occlusive microvasculopathy and leads

to vision loss.[12] However, the temporal relationship between the appearance of retinal and vascular pathology has not been established conclusively in humans.

The advent of optical coherence tomography angiography (OCT-A) for high-resolution imaging of the retinal microvessels has allowed for a more detailed understanding of microvascular pathology, especially capillary dropout, and expanded the knowledge provided by the Collaborative Ocular Melanoma Study reports, which used fluorescein angiography.[13–16] In particular, a loss of capillaries in the superficial and deep capillary plexuses of the parafoveal area has been reported after ^{125}I-plaque brachytherapy.[13–16] However, because the development of vasculopathy has only been compared with measures of visual acuity, a measure of foveal function, there is a need for visual field testing within the macula to better characterize the time course for neuronal dysfunction and its relationship to microvasculopathy.

Here, we leverage readouts of visual acuity, automated threshold perimetry, digital fundus photography, OCT, and OCT-A to determine the effect of time from radiation therapy, dose, and spatial location within the retina on radiation retinopathy. Moreover, we incorporate each patient's OCT-A scan into our dosimetry models to calculate radiation dose distributed to the same macular locations in which vascular and neuronal readouts were obtained.

Methods

Study Subjects

Patients with uveal melanoma treated with ^{125}I-plaque brachytherapy were consecutively enrolled from the Retina and Vitreous Clinic at the University of Iowa Hospital and Clinics. All subjects provided written informed consent before screening or initiation of any procedures. The study protocol was approved by the University of Iowa Institutional Review Board for Human Use and followed the tenets of the Declaration of Helsinki. Patients were enrolled and imaged once at time points ranging from 2 weeks to 13 years after plaque removal. Exclusion criteria included melanoma involving the central macula, exudative AMD, severe macular edema that interfered with OCT retinal layer segmentation, cataract interfering with the quality of retinal imaging, restriction in ocular motility, severe central vision loss (worse than 20/200 and/or inability to track a central fixation point), glaucoma with field loss within the central 10°, or disease of the contralateral eye preventing its use as a within-subject control. The presence of diabetic retinopathy was not an exclusion factor. Complete sets of OCT-A scans and visual field testing were obtained in 47 patients. Of these 47 patients, interpretable data with all testing modalities were generated in 25 patients and used for further analysis. Six patients were excluded after testing owing to significant image artifact, especially motion artifact, excessive blinking, and vitreous opacities interfering with image quality; 10 because of technical inability to segment the OCT volume scans owing to severe macular edema or wet macular degeneration; 3 owing to unavailable visual fields; and 3 owing to unavailable radiation dosimetry records.

Control subjects were recruited by advertisements within the University of Iowa Hospitals and Clinics. Control subjects were prescreened by OCT (Cirrus HD-OCT 5000, Carl Zeiss Meditec, Inc. Dublin, CA) for normal retinal nerve fiber and ganglion cell layer thickness. Subjects were considered normal if their retinal nerve fiber layer thickness (by 36 mm^2 Optic Disc Cube 200 × 200 scan) and ganglion cell layer (by 36 mm^2 Macular Cube 200 × 200 scan) fell within the 5th and 95th percentile range of the age-matched normative database. OCT-A scans were obtained in both eyes of 16 normal control subjects. The variability of the intereye ratio between control subjects was calculated by coefficient of variation (mean ± SD).

Acquisition and Analysis of OCT/Angiography Scans

A single 6 × 6 mm^2 OCT-A scan centered on the foveal avascular zone (FAZ) was acquired in both eyes of each subject (Optovue XR Avanti System, Optovue, Inc., Fremont, CA). The size of the superficial retinal FAZ and the percent vessel density of the parafoveal region, defined as a 300-µm ring around the FAZ demarcated by the device software (AngioVue, v.2018.0.0.18, Optovue, Inc.), were automatically calculated and reported by the device software.

OCT-A images were processed manually in ImageJ[17] (v. 1.52p; National Institutes of Health, Bethesda, MD) to optimize the signal-to-noise ratio, and to equally weight large and small vessels, as follows (Supplementary Fig. 1). First, the scan of the treated eye was histogram matched (Bleach Correction, Histogram Matching[18]) to the scan of its fellow eye. Next, the background signal, determined by sampling the signal in the FAZ,[19,20,21] was subtracted from the total image. The vasculature was sharpened using the Tubeness[22] plugin (σ = 1.75). Then, images were binarized using the mean thresholding method, so that vessels were represented by white pixels on a black background. Finally, the image was skeletonized (Binary > Skeletonize) to equally weight all vessels.[23] The number of white pixels was counted and divided by the total number of pixels to yield vessel skeleton density.

Fractal dimension[19,23–28] and lacunarity,[21,29] quantitative measures of vascular network integrity, were calculated using the ImageJ plugin FracLac (Sliding Box Lacunarity Analysis function).[30] Processed images were opened in the plugin and analyzed using the following parameters: 20 sizes, default sampling sizes, minimum size 5 pixels, maximum percent of image 0, and smooth box counting filter on. These settings were selected following an iterative analysis of data from the control group.

Separately, pseudocolored, two-dimensional macular maps of avascular (red), hypovascular (orange), and normal (green) vascular areas were generated using a novel deep learning-based approach.[31] Briefly, the retinal layers were first segmented in the corresponding SD-OCT volumes using a previously developed graph-based layer segmentation algorithm and included the retinal nerve fiber layer to the inner plexiform layer. OCT-A en face images were generated using the maximum intensity from the corresponding SSADA data, then unified to a 480 × 480-pixel resolution. A U-Net–derived deep neural network with VGG11-like encoder[32,33] was trained to predict the three regions from the OCT-A en face images. This network outputs independent probabilities for each of the grades over the entire scan area.

Spectral domain-OCT volume scans were segmented to provide inner and total retinal thickness of the area imaged by OCT-A. Scans were processed using retinal segmentation methods described previously,[34,35] which yield a continuum of values across the imaged area. The mean thickness for the

Investigative Ophthalmology & Visual Science

inner retinal layer (including the retinal nerve fiber layer to the outer border of the inner plexiform layer) and the total retinal thickness were calculated for the macula of each eye.

All OCT-derived measurements were reported as the ratio of the treated eye to the fellow eye. In a randomly selected 50% of the control subjects, the ratios were calculated as right over left, and as left over right in the remaining 50%. For each measurement of vascular and neuronal pathology, a data point was defined as normal if within the range of the mean ± 3 SDs of ratio values in normal subjects.

Static Automated Perimetry

The Swedish Interactive Threshold Algorithm standard automated perimetry was performed with a Humphrey Field Analyzer (Humphrey Field Analyzer Model 750i, Carl Zeiss Meditec, Inc., Dublin, CA) using the 10-2 protocol (2° grid spacing of stimuli across a 10° radius visual field using a size III light) on the treated eye. All patients had reliable visual fields, defined as fewer than 33% of fixation losses, false-positive results, and false-negative results. For analysis, a field was defined as abnormal if the mean deviation and/or pattern SD had a *P* value of 5% or less from the analyzer's built-in set of age-matched normative data.

Visual Acuity

The best-corrected Early Treatment Diabetic Retinopathy Study (ETDRS) visual acuity of the treated eye was measured at the time of scan acquisition and compared with visual acuity at the time of diagnosis. An abnormal logMAR visual acuity at scan acquisition was defined as a loss of two or more ETDRS lines compared with the time of tumor diagnosis.

Qualitative Clinical Assessment of Radiation Retinopathy

Digital color fundus photographs were taken with a Topcon TRC 50-DX retinal camera (Topcon, Tokyo, Japan), which generated an image size of 2392 × 2048 pixels from an OIS full frame 36 mm sensor, with an effective resolution of 4.89 megapixels. The images were evaluated and viewed with Zeiss Forum software (Carl Zeiss Meditec, Inc.) using a 27-inch, 5120 × 2880-pixel built-in retina display (Apple Corp, Cupertino, CA).

Two expert examiners (EMB, RHK) independently evaluated the presence of radiation retinopathy within the macula between the superior and inferior temporal retinal arteriole arcades. The examiners were masked to the treatment details and time point of the radiation treatment. The images were classified as abnormal if any of the following features of radiation retinopathy were detected within the macula (defined by the temporal vascular arcades): intraretinal hemorrhages, microaneurysms, sclerotic vessels, telangiectatic vessels, cotton wool spots, or hard exudates.

Further, OCT volume scans (OCT Spectralis, Heidelberg Engineering, Franklin, MA) were evaluated (by EMB) for radiation retinopathy. Scans were classified as abnormal if any of the following features of radiation retinopathy were detected: intraretinal or subretinal fluid or abnormal retinal thickening.

Dosimetric Calculations

The average dose to the imaged macula area was calculated for each patient with the ocular brachytherapy planning software Plaque Simulator (v.6.6, EyePhysics, LLC, Los Alamitos, CA). For each patient, a three-dimensional model was constructed using their OCT-A scan, fundus photograph, tumor dimensions, and radiation prescription. Total dose was calculated at 81 points across the 6 × 6 mm^2 scan and averaged to yield the mean macula dose. Additional, commonly reported dose characteristics (dose to the prescription point, tumor apex, optic disc, and foveola) were obtained from each patient's clinical radiotherapy treatment plan, calculated using TG-43 methods.[36]

Statistical Analysis

Spearman correlation (two-tailed, 99% confidence interval) was used to identify relationships between each outcome measure. Fisher's exact test (two-tailed, 99% confidence interval) was used to identify significant differences between measures grouped by time after radiotherapy. Kruskal-Wallis ANOVA with Dunn's multiple comparisons test was used to compare bevacizumab treatment groups. Area under the receiver operator characteristic curves for radiation retinopathy, defined by either an abnormal visual field test or a digital fundus photograph with signs of radiation retinopathy, was calculated for each outcome measure. All statistical calculations were performed using GraphPad Prism (v.8.2.1 for Windows, GraphPad Software, San Diego, CA).

Results

Patient Population

Of the 47 patients enrolled, complete datasets were obtained from 25 (Fig. 1). The average age of the patients was 61 years, and 68% were male (Table 1). In the patient population, 24% had hypertension, 16% had diabetes mellitus, and 8% had both diabetes and hypertension. The average time from treatment was 33 months. All patients had tumors involving the choroid, with 20% involving the ciliary body and 16% the peripapillary region (Supplementary Table 1). A prophylactic bevacizumab injection was given at plaque removal in 52% of patients (Supplementary Table 2). The average dose to the macula was 48 Gy. The mean age of the 16 normal control patients was 49 years, 44% were males, and 13% had hypertension (Table 1).

Method Validation

The normal range for each test was calculated as the mean ± 3 SDs in the normal control group (Table 2). The variability (coefficient of variation) of the intereye ratio was 5% or less for vessel skeleton density, fractal dimension, lacunarity, inner retinal layer thickness, total retinal thickness, and normal area (data not shown). Variability was highest for avascular area, hypovascular area, and FAZ area owing to asymmetry between normal eyes.

To further validate our methods, receiver operator characteristic curves for each measurement were calculated using an abnormal visual field test or presence of features of retinopathy on fundus photography as criteria for presence or absence of radiation retinopathy (Table 3). The areas under the curve (AUCs) between the two diagnostic factors

Investigative Ophthalmology & Visual Science

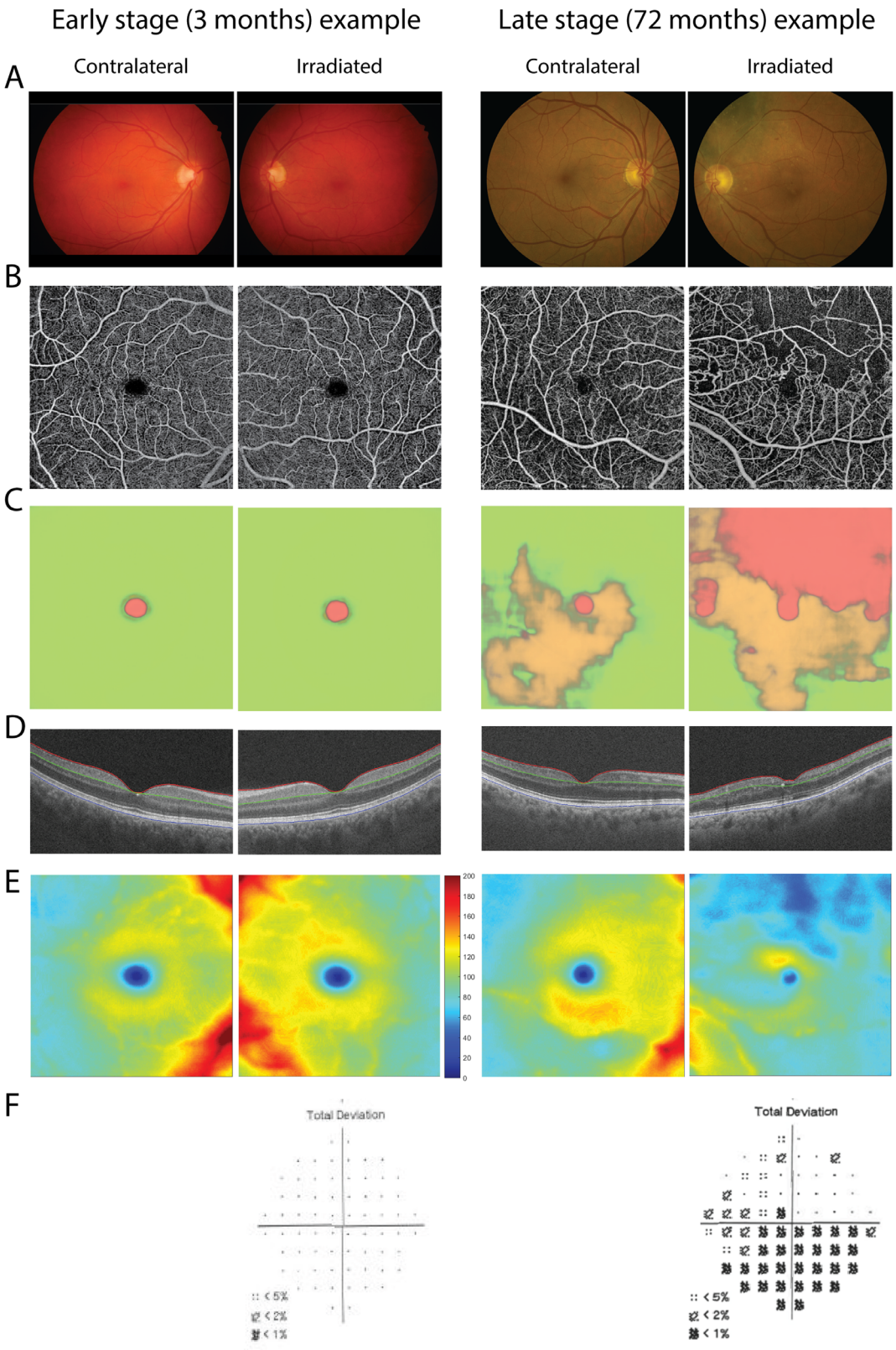

Figure 1. Imaging modalities to assess radiation retinopathy. Representative images from treated and fellow eyes of an early stage patient (3 months after treatment, *left*) and late-stage patient (72 months after treatment, *right*). **(A)** Digital fundus photographs centered on the fovea. **(B)** A 6 × 6 mm^2 OCT-A scans (Optovue) of the superficial retinal microvasculature. Scans were used to calculate FAZ size, parafoveal density, vessel skeleton density, fractal dimension, and lacunarity. **(C)** Maps of vascularity with avascular (*red*), hypovascular (*orange*), and normal (*green*) areas determined by a trained neural network. **(D)** OCT-B scans (Optovue) selected from the segmented volume scan used to calculate retinal thickness maps **(E)** using custom segmentation methods. *Red lines* are at the inner limiting membrane, *green* segmentation lines are at the posterior boundary of the inner plexiform layer, and *blue lines* are at the posterior boundary of the retinal pigment epithelium complex. Scale bars given in µm. **(F)** Results of 10-2 visual field testing of the corresponding 6 × 6 mm^2 area in the irradiated eye showing the probability plot compared with normal eyes.

Table 1. Subject Demographics

Features	Patients, No. (%), $n = 25$	Controls, No. (%), $n = 16$
Age (years), median (mean, range)	61 (61, 28–83)	47 (49, 35–67)
Caucasian race	25 (100)	16 (100)
Sex		
Male	17 (68)	7 (44)
Female	8 (32)	9 (56)
Medical history		
Hypertension	6 (24)	2 (13)
Diabetes mellitus	4 (16)	0 (0)
Diabetes mellitus and hypertension	2 (8)	0 (0)
Diabetes mellitus and diabetic retinopathy*	1 (4)	0 (0)
LogMAR visual acuity, median (mean, range)		
Time of diagnosis	0.04 (0.06, –0.10–0.40)	NA
Time of study visit	0.04 (0.12, –0.08–1.00)	NA
Months post-treatment, median (mean, range)	18 (33, 0.25–143)	NA

* Diagnosis was determined by a single microaneurysm in each eye seen on digital fundus photograph.

Table 2. Normative Range for Outcome Measures

Measurement	Right Eye, $\mu \pm 3\sigma$	Left Eye, $\mu \pm 3\sigma$	Intereye Ratio,* μ ($\mu - 3\sigma, \mu + 3\sigma$)
FAZ area	0.256 ± 0.355	0.253 ± 0.348	1.051 (0.346, 1.756)
Parafoveal vessel density	53.57 ± 14.56	55.42 ± 9.29	1.040 (0.780, 1.300)
Vessel skeleton density	12.215 ± 0.849	12.246 ± 0.861	1.003 (0.955, 1.051)
Fractal dimension	1.042 ± 0.009	1.043 ± 0.007	1.000 (0.995, 1.005)
Lacunarity	0.051 ± 0.006	0.050 ± 0.005	0.9886 (0.834, 1.144)
Normal area	0.969 ± 0.021	0.972 ± 0.020	0.996 (0.973, 1.018)
Hypovascular area	0.025 ± 0.046	0.030 ± 0.099	1.056 (0.002, 2.110)
Avascular area	0.017 ± 0.012	0.016 ± 0.013	1.057 (0.554, 1.559)
Inner retinal layer thickness	0.108 ± 0.021	0.110 ± 0.021	0.996 (0.926, 1.066)
Total retinal thickness	0.301 ± 0.037	0.302 ± 0.039	0.998 (0.965, 1.030)
Visual field mean deviation (dB)†	NA	NA	NA

μ, mean; σ, SD.
* Mean and SD calculated using intereye ratios (randomly assigned 8 OD/OS and 8 OS/OD for total of 16 control subjects).
† Visual fields are obtained in each patient's treated eye only, as results are automatically compared with the manufacturer's age-matched normative database.

Table 3. AUC*

Measurement	AUC	
	Visual Field	Retinopathy Diagnosis
Vascular pathology		
FAZ area	0.808	0.771
Parafoveal density	0.769	0.813
Vessel skeleton density	0.776	0.868
Fractal dimension	0.789	0.875
Lacunarity	0.750	0.819
Normal area	0.878	0.840
Hypovascular area	0.776	0.924
Avascular area	0.891	0.861
Retinal pathology		
Inner retinal layer thickness	0.897	0.604
Total retinal thickness	0.827	0.569
Visual outcomes		
ΔlogMAR visual acuity†	0.641	0.795
Visual field mean deviation (dB)	NA	0.754
Clinical assessment		
Fundus photograph evaluation‡	0.715	NA

* ROC curves were calculated based on either abnormal visual field or diagnosis of radiation retinopathy by fundus photography.
† ΔlogMAR visual acuity is defined as the difference between visual acuity at time of diagnosis and time of study visit.
‡ Color fundus photographs were evaluated for features of radiation retinopathy within the central 10° of the macula by two independent physician experts masked to the treatment details and time point after treatment.

Investigative Ophthalmology & Visual Science

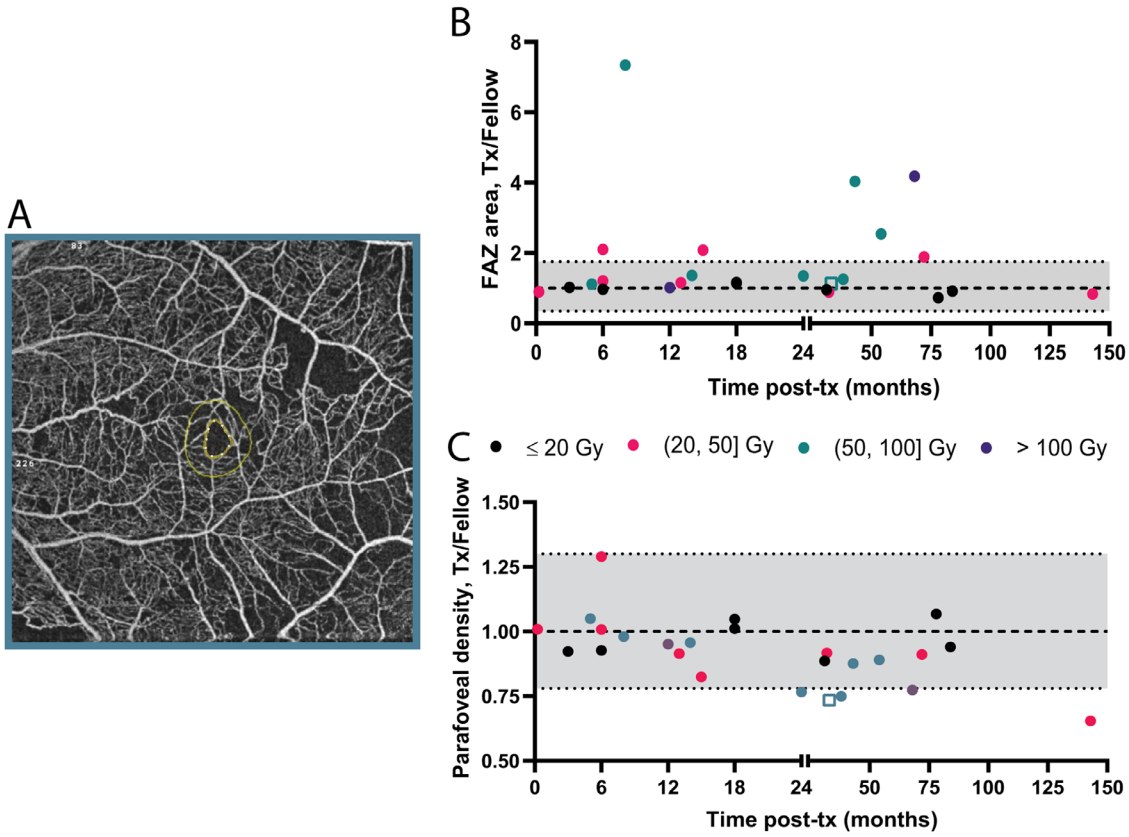

Figure 2. FAZ area and parafoveal density in patients after ^{125}I-plaque brachytherapy. **(A)** Representative 6 × 6 mm^2 OCT-A scan used to determine the FAZ area (*center ring*) and parafoveal density (*outer ring*) using the Optovue software. **(B)** Ratio of FAZ area in the treated (Tx) to the normal control (Fellow) eye for 25 patients as a function of time after treatment. **(C)** Ratio of parafoveal density as determined in **(B)**. For **(B** and **C)**, data points are color coded by mean dose to the macula, and the normal range for intereye asymmetry (3 SD) determined from a control group of normal subjects is shown in grey. Data point corresponding to image indicated by an *open square*.

were similar for most measures. Most vascular measures had higher AUCs by radiation retinopathy diagnosis; similarly, the AUCs for retinal thickness were higher when abnormal visual field was used as the diagnostic factor. The highest AUCs were seen for our novel vascularity calculations, and inner retinal layer thinning with abnormal visual field as the diagnostic factor (AUC = 0.897).

Radiation Microvasculopathy by OCT-A

To identify the most sensitive OCT-A metric to detect early radiation retinopathy, we analyzed images from the 13 patients that were imaged within the first 2 years after brachytherapy. Parafoveal density and FAZ area, despite having been previously reported as early indicators of vascular pathology,[15] were abnormal in 1 of 13 and 2 of 13 patients, respectively (Fig. 2, Table 4). The structure and organization of the microvessel network, described by vessel skeleton density (Fig. 3A–C), fractal dimension (Fig. 3A, B, D), and lacunarity (Fig. 3A, B, E), was abnormal in three, three, and one patient, respectively. By our novel pixel-based deep learning approach,[31] we identified four patients with abnormal hypovascularity (Fig. 4A, B, D), avascularity (Fig. 4A, B, E) and normal vascularity (Fig. 4A, B, C).

For the 12 patients imaged at 2 years or later after brachytherapy, pathology was detected by every measure. Parafoveal density and FAZ area were the least frequent abnormalities (42% and 33%, respectively; Table 4). All other measures of vascular density decreased similarly over time, with the greatest number of patients (67%) deemed abnormal by our machine learning-derived measures of vascularity. Lacunarity was the only measure of vascular abnormality that was significantly worse in the group imaged more than 2 years after radiation treatment compared with the group imaged less than 2 years after radiation treatment ($P = 0.011$ by Fisher's exact test; Table 4).

Change in Retinal Thickness by OCT Volume

Because a change in retinal thickness is a clinical marker of radiation retinopathy,[37,38] we segmented OCT volume scans to measure the thickness of the inner retinal layers and the total retina in the same area of the macula that was analyzed for vascular abnormality (Fig. 5A–C). In 5 of the 13 patients who were imaged within the first 24 months after brachytherapy, retinal thickening as a result of inner retinal thickening, edema, or fluid collections was present. Abnormal thinning was observed in one patient who was imaged within the first 2 years after brachytherapy (Fig. 5D–E). There was no overlap between abnormal retinal thickness and abnormal vascular features in this time period.

Table 4. Percentage of Subjects with Vascular and Retinal Pathology

Measurement	Abnormal,* *n* (%)			*P* Value†
	< 24 Mo	≥ 24 Mo	Overall‡	
Vascular pathology				
FAZ area	2 (15)	4 (33)	6 (24)	ns
Parafoveal density	1 (8)	5 (42)	6 (24)	ns
Vessel skeleton density	3 (23)	7 (58)	10 (40)	ns
Fractal dimension	3 (23)	7 (58)	10 (40)	ns
Lacunarity	1 (8)	7 (58)	8 (32)	0.011
Normal area	4 (31)	8 (67)	12 (48)	ns
Hypovascular area	4 (31)	7 (58)	11 (44)	ns
Avascular area	4 (31)	8 (67)	12 (48)	ns
Retinal pathology				
Inner retinal layer thinning	1 (8)	6 (50)	7 (28)	0.030
Total retinal thinning	1 (8)	5 (42)	6 (24)	ns
Inner retinal layer thickening§	5 (38)	4 (33)	9 (36)	ns
Total retinal thickening	5 (38)	2 (17)	7 (28)	ns
Visual outcomes				
ΔlogMAR visual acuity‖	2 (15)	2 (17)	4 (16)	ns
Visual field mean deviation (dB)¶	5 (38)	8 (67)	13 (52)	ns
Clinical assessment				
Fundus photograph evaluation#	6 (46)	10 (83)	16 (64)	ns
Volumetric OCT evaluation**	2 (15)	7 (58)	9 (36)	0.041

Data are presented for the entire cohort and for subgroups of patients imaged before 24 months ($n = 13$) and after 24 months after radiotherapy ($n = 12$).

* A measure is called abnormal if it falls outside of the normal range, defined by the control ratio $\mu \pm 3\sigma$ in Table 2.

† Calculated for comparison of <24-month and ≥24-month groups by Fisher's exact test.

‡ Percent calculated for the entire ($n = 25$) cohort; describes the number of subjects abnormal by the last time point.

§ Thickening defined as a thickness ratio that falls above the upper confidence limit of the defined normal range.

‖ Abnormal ΔlogMAR is defined as a loss of two or more Snellen lines since time of diagnosis.

¶ Abnormal visual field defined by a mean deviation and/or pattern SD of $P \leq 5\%$.

Radiation retinopathy diagnosis determined by physician evaluation of the central 10° of the macula seen in color fundus photographs.

** Radiation retinopathy diagnosis determined by physician evaluation of volumetric OCT scans of the macula taken as standard of care on the same day as the color fundus photographs.

For the 12 patients seen at 2 years or later, 50% had a decreased thickness of the inner retina, and 33% had abnormally increased inner layer thickness (Table 4). Inner retinal layer thinning was also significantly different between the two groups ($P = 0.030$ by Fisher's exact test; Table 4). All patients with diminished retinal thickness had abnormal vascular features, consistent with decreased capillary density.

Loss of Visual and Retinal Function by Standard Automated Perimetry and Visual Acuity

Loss of neuronal function was measured by visual field testing of the central 10° of the retina (Fig. 6A–B), which corresponds with the area analyzed by the other testing modalities. In the first 2 years after radiotherapy, 38% of patients had abnormal visual fields (Table 4). Two patients with abnormal visual fields also had abnormal vascular features, whereas two patients with abnormal visual field had abnormal retinal thickness.

Because the ETDRS visual acuity test has been the standard clinical measurement of vision loss in studies of radiation retinopathy,[5] we measured best-corrected visual acuity and compared it with visual acuity at the date of diagnosis (Fig. 6C). Only two patients seen in the first 2 years after brachytherapy had an abnormality by this measure.

For the 13 patients tested at or after 2 years after brachytherapy, 67% had abnormal visual fields and 17% abnormal vision by ETDRS (Table 4). All patients with abnormal visual fields also had abnormal vascular features; all but one had abnormally thinned retinas.

Retinopathy Diagnosis by Qualitative Analysis of Digital Fundus Photography and OCT

To compare the efficacy of our measurements with qualitative clinical assessment, two ophthalmologists independently evaluated digital fundus photographs for evidence of radiation retinopathy within the central 10° of the retina. There was 96% (24/25) agreement between the two reviewers. Of the patients tested within the first 2 years after radiotherapy, 46% met criteria for radiation retinopathy (Table 4). Four of these patients had abnormal vascular features by OCT-A, three had an abnormal visual field, one had abnormal thinning of the inner and total retina, and four had abnormal thickening of the inner and total retina. For the 12 patients seen 2 years or later after brachytherapy, 83% presented features of radiation retinopathy by fundus photography. Eighty percent of these patients also had abnormal vascular features by OCT-A, 70% had abnormal retinal thinning by OCT, and 80% had abnormal visual fields.

Next, OCT scans taken as a part of the routine clinic evaluation on the same date as the color photographs at each patient visit were reviewed for features of radiation retinopathy. All patients with radiation retinopathy by OCT had been similarly identified features by fundus photograph;

Investigative Ophthalmology & Visual Science

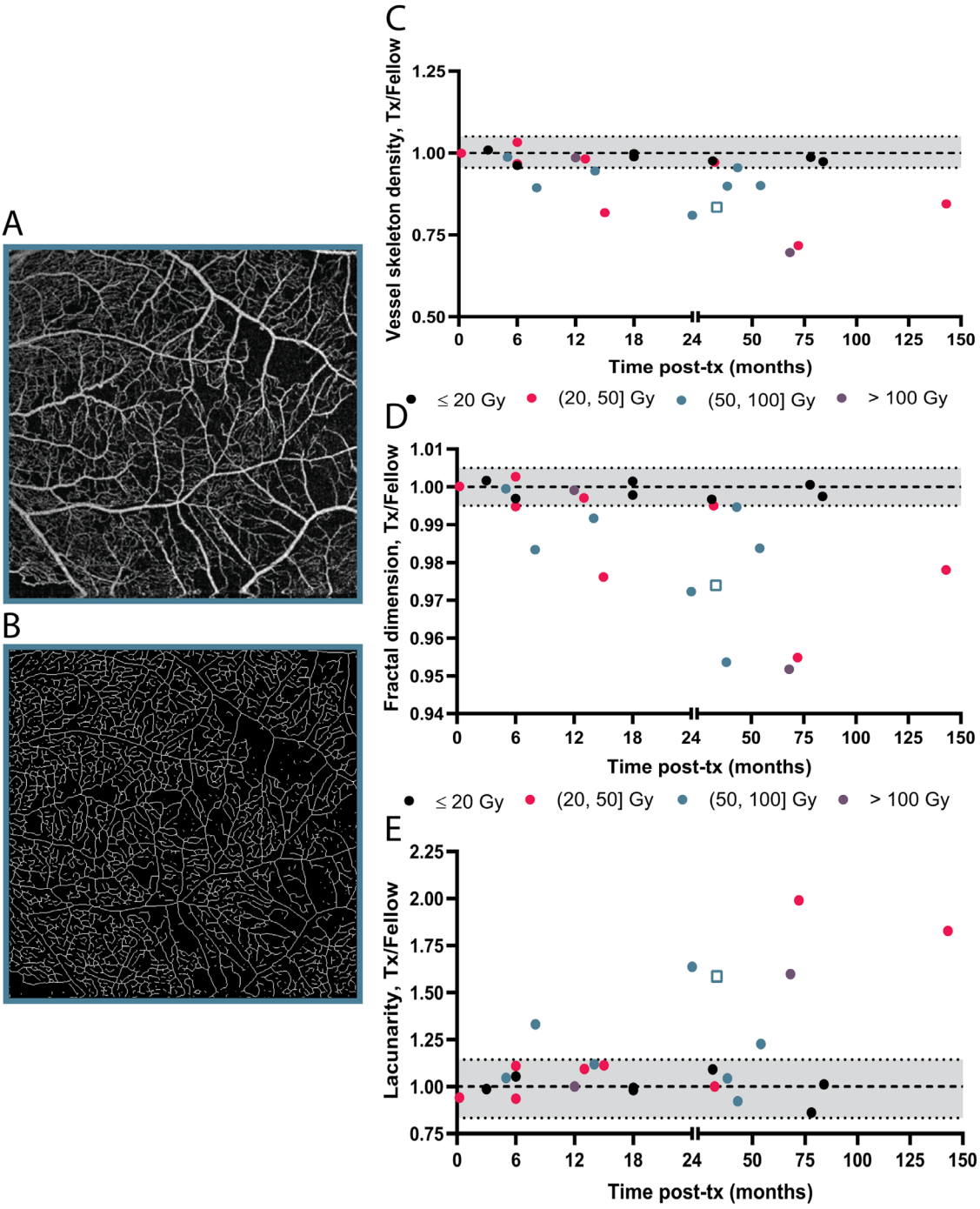

Figure 3. Vessel skeleton density, fractal dimension, and lacunarity in patients after ^{125}I-plaque brachytherapy. **(A)** Representative 6 × 6 mm^2 OCT-A scan and **(B)** processed image after histogram matching, subtracting background noise defined by the FAZ area signal, binarizing, and skeletonizing the raw OCT-A scan in ImageJ. **(C)** Ratio of pixel-measured vessel skeleton density in the treated (Tx) to the normal control (Fellow) eye are plotted as a function of time from treatment. **(D)** Ratio of fractal dimension and **(E)** lacunarity determined as in **(C)**. For **(C–E),** data points are color coded by mean dose to the macula, and the normal range for intereye asymmetry (3 SD) determined from a control group of normal subjects is shown in grey. Data point corresponding to image indicated by an *open square*.

seven patients presented features of radiation retinopathy in their fundus photographs but not their OCT scans (intraretinal hemorrhage, sclerotic vessels, and/or cotton wool spots). Diagnosis of radiation retinopathy by OCT was significantly more common in patients seen at later time points ($P = 0.041$ by Fisher's exact test; Table 4).

Timeline to Vascular and Retinal Pathology

Next, we plotted the cumulative fraction of subjects classed as abnormal by time, to identify a temporal course of pathology (Fig. 7). Vascular changes and neuronal dysfunction were detected in patients imaged as early as 6 months after

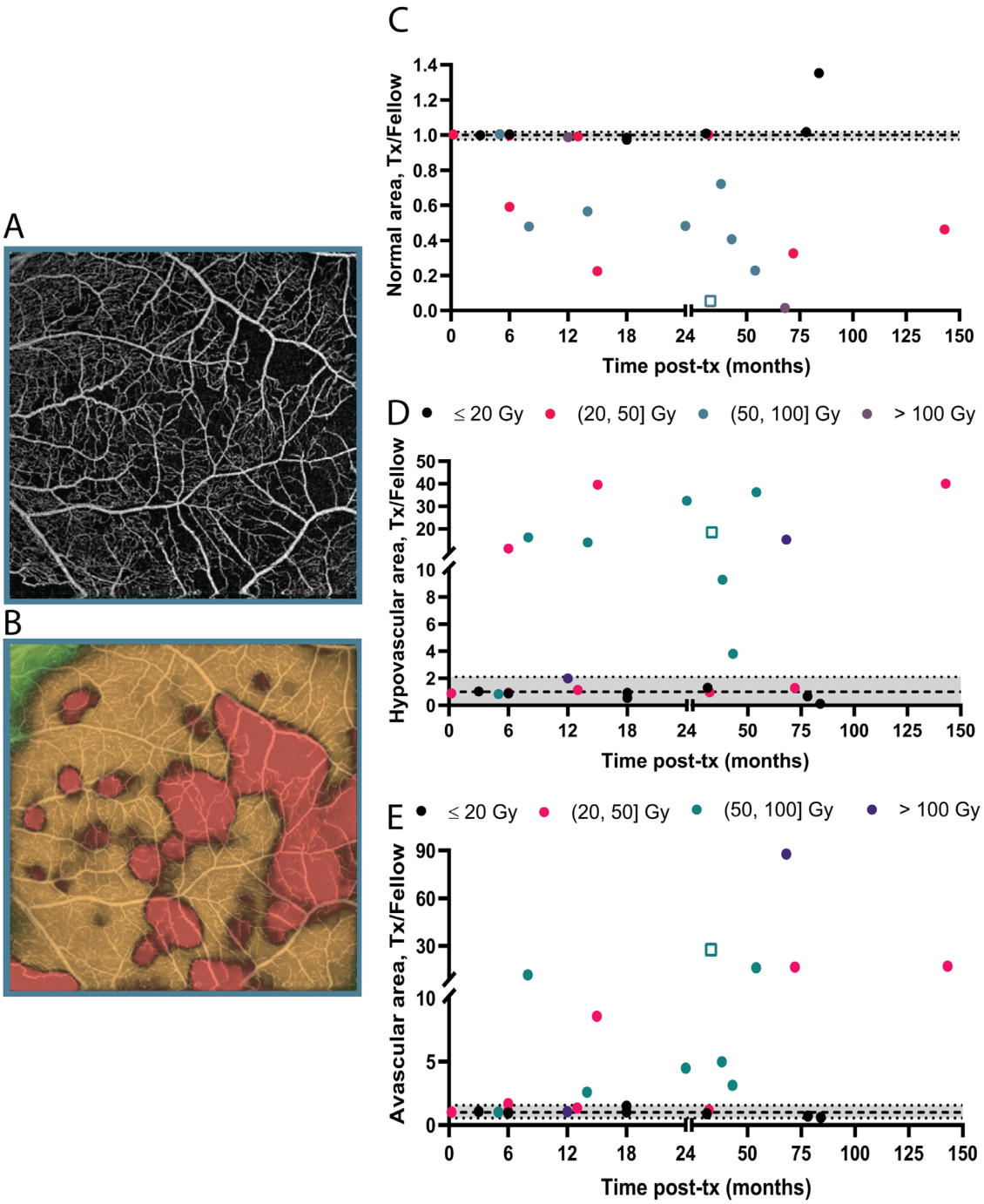

Figure 4. Regional changes in vascularity in patients after ^{125}I-plaque brachytherapy. **(A)** Representative 6 × 6 mm^2 OCT-A scan and **(B)** map of graded vascularity that distinguish avascular (*red*), hypovascular (*orange*), and normal areas (*green*). The average probability value for each category is calculated. **(C)** Ratios of normal areas in the treated (Tx) and the normal control (Fellow) eye are plotted are plotted as a function of time from treatment. **(D)** Ratios of hypovascular and **(E)** avascular areas determined as in **(C)**. For **(C–E)** data points are color coded by mean dose to the macula, and the normal range for intereye asymmetry (3 SD) determined from a control group of normal subjects is shown in grey. Data point corresponding to image indicated by an *open square*.

brachytherapy. Increased thickness of the inner retina was seen as early as 3 months after brachytherapy, whereas thinning was seen in only one patient imaged within the first 2 years after treatment. Signs of radiation retinopathy were detected by fundus photography in one patient imaged at 3 months; by qualitative analysis of OCT at 8 months. Importantly, by the latest time point, more patients were classed as having abnormalities by fundus photograph evaluation (64%), loss of visual function by 10-2 visual field (52%), and deep learning-derived vascularity (48%), whereas far fewer subjects were classed abnormal by FAZ area, parafoveal density, and change in visual acuity by ETDRS (24%, 24%, and 16%, respectively). Of note, with the exception of lacunarity ($P = 0.011$), which measures the disruption of pattern

Investigative Ophthalmology & Visual Science

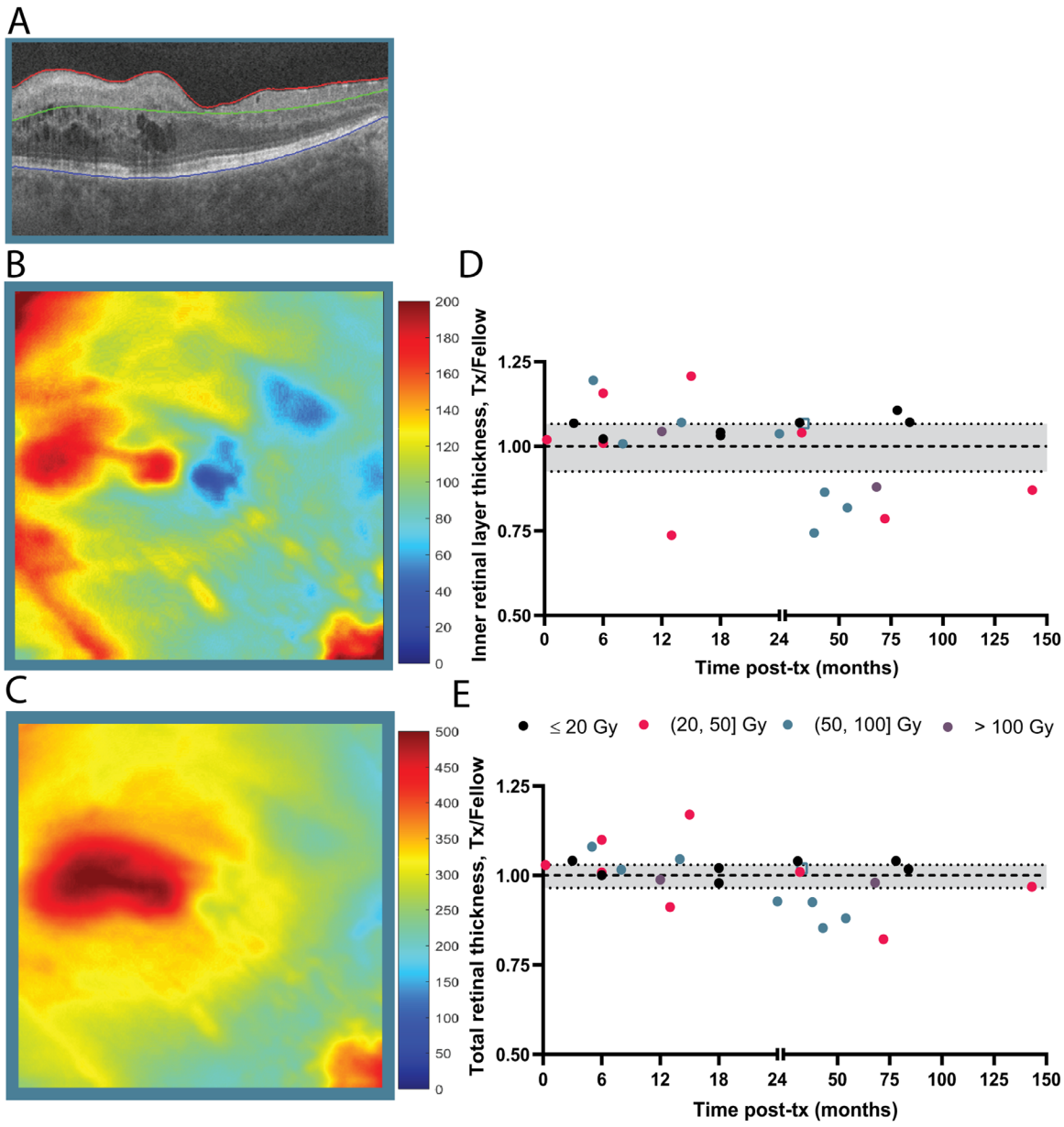

Figure 5. Inner retinal layer and total retinal thickness in patients after ^{125}I-plaque brachytherapy. **(A)** Representative OCT-B scan and **(B)** map of inner layer and **(C)** total retinal thickness provided by custom volume segmentation methods. A mean thickness value calculated from a continuum of voxel-wise thickness values is reported. **(D)** Ratios of inner retinal layer thickness over the 6 × 6 mm^2 area in the treated (Tx) divided by the normal control (Fellow) eye are plotted as a function of time from treatment. **(E)** Ratios of total retinal thickness determined as in **(D)**. For **(D–E)** data points are color coded by mean dose to the macula, and the normal range for intereye asymmetry (3 SD) determined from a control group of normal subjects is shown in *grey*. Data points above the normal range are classed as having retinal thickening, whereas points below the normal range have retinal thinning. Data point corresponding to image indicated by an *open square*. Scale bars for **(B–C)** given in micrometers.

regularity by the appearance of gaps in the vascular network, no significant differences between the various approaches to detect microvasculopathy were seen in the cumulative analysis (Fisher's exact test; Table 4).

To substantiate the relationships between the readouts for vascular and neuronal pathology, we generated a Spearman correlation matrix (Supplementary Fig. 2). Because both retinal thinning and thickening are expected to correlate with vascular retinal pathology, the absolute difference between each patient's retinal thickness ratio and the mean ratio of the age-matched control group was calculated, as described previously.[28] As anticipated, the readouts of vascular abnormality strongly correlated with one another, for example, the vessel skeleton density with fractal dimension, lacunarity, normal area, hypovascular area, and avascular area ($P < 0.001$). Moreover, absolute changes in the inner retinal layer thickness correlated with visual sensitivity by visual field ($P = 0.027$). Although a change in logMAR visual acuity correlated with several vascular measures, such as the FAZ area ($P = 0.016$), it did not correlate with significance with absolute change in inner layer or total retinal thickness ($P = 0.150$ and 0.326, respectively). Neuronal function assessed

Investigative Ophthalmology & Visual Science

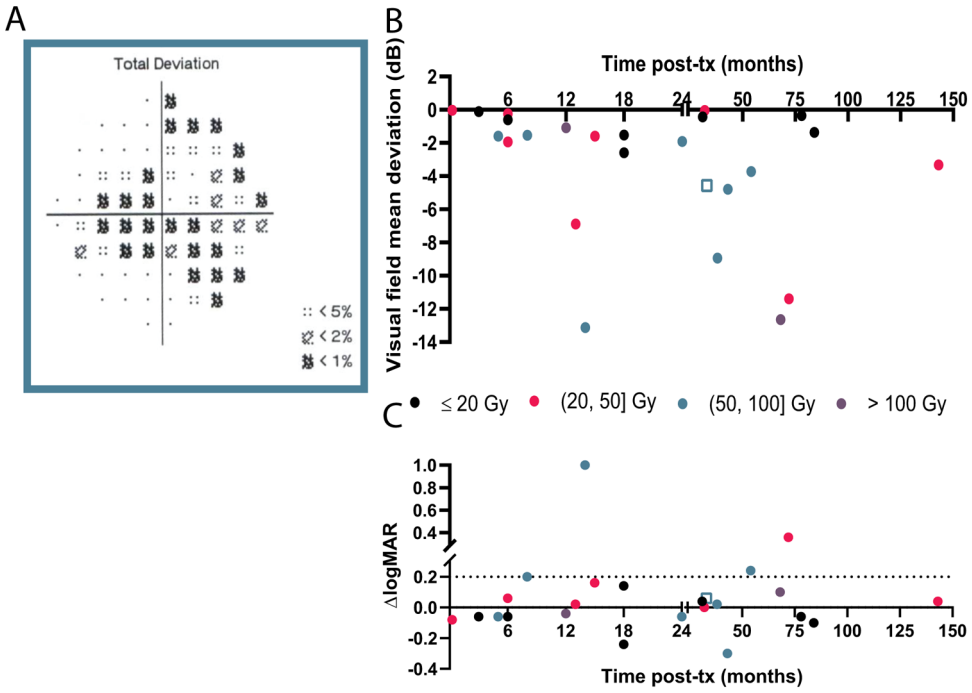

Figure 6. Visual field defects in patients after ^{125}I-plaque brachytherapy. **(A)** Representative result of 10-2 visual field testing probability plot of decibel deviation at each test location from an age-matched database. **(B)** Mean deviation in decibels over the 10-2 visual field of the treated eye plotted as a function of time from treatment. **(C)** Change in Snellen visual acuity by logMAR in the treated eye since time of tumor diagnosis, plotted as a function of time from treatment. Points on or above the dotted line indicate abnormal subjects (change in two or more lines since time of diagnosis). Data point shown in **(A)** indicated as an *open square* in **(B)** and **(C)**.

Table 5. Comparison of Outcome Measures in Relation to Bevacizumab Treatment

	Comparison		
Measurement	**No Injection vs At Removal Only**	**No Injection vs Multiple Injections**	**At Removal Only vs Multiple Injections**
Time post-surgery (months)	0.004	ns	0.031
Vascular pathology			
FAZ area	ns	ns	ns
Parafoveal density	ns	ns	ns
Vessel skeleton density	ns	ns	0.011
Fractal dimension	ns	ns	0.009
Lacunarity	ns	0.011	0.044
Normal area	ns	0.005	0.010
Hypovascular area	ns	ns	0.031
Avascular area	ns	0.008	0.004
Retinal pathology			
Inner retinal layer thickness	ns	ns	ns
Total retinal thickness	ns	ns	ns
Visual outcomes			
ΔlogMAR visual acuity	ns	0.011	0.005
Visual field mean deviation (dB)	ns	ns	ns

The *P* values are listed for the comparison of no injection ($n = 6$), single injection at plaque removal ($n = 10$), and multiple prophylactic injections ($n = 9$) groups.

by visual field strongly correlated with all measures except visual acuity and absolute change in total retinal thickness.

Effect of Bevacizumab Treatment on the Development of Vascular and Retinal Pathology

To examine the effects of bevacizumab treatment on retinal dysfunction, we performed a Kruskal–Wallis ANOVA with Dunn's multiple comparisons test of three treatment groups—no bevacizumab ($n = 6$), injection at time of plaque removal only ($n = 10$), and multiple prophylactic injections ($n = 9$; Fig. 8, Table 5). Of note, patients without bevacizumab and those who were treated after plaque removal were imaged at an average time interval of 51 and 46 months, respectively, after treatment, whereas those with one treatment at plaque removal only were seen after 10 months

Investigative Ophthalmology & Visual Science

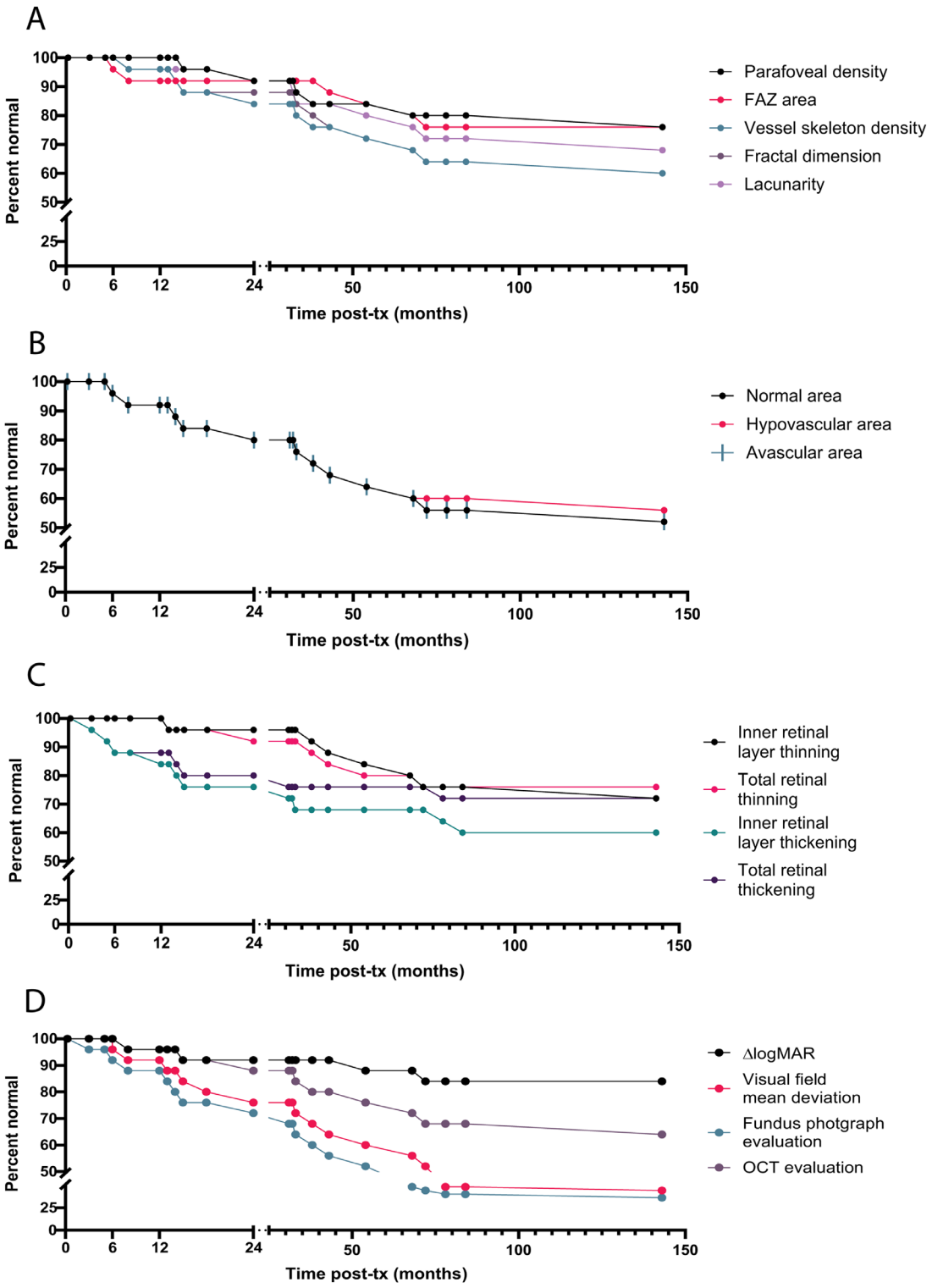

Figure 7. Cumulative time course of visual field defects, retinal and microvascular pathology after ^{125}I-plaque brachytherapy. Cumulative percentage of patients classed as normal by **(A)** vascular pathology derived from Optovue software (FAZ area, parafoveal density) or processing in ImageJ (vessel skeleton density, fractal dimension, lacunarity), **(B)** vascular pathology derived from image processing by pixel-based deep learning, **(C)** thinning and thickening of inner and total retinal layers, **(D)** 10-2 visual field testing (HVF; mean deviation or pattern deviation $P < 0.05$), Snellen visual acuity (ΔlogMAR), and grading of digital fundus photographs and OCT scans for radiation retinopathy.

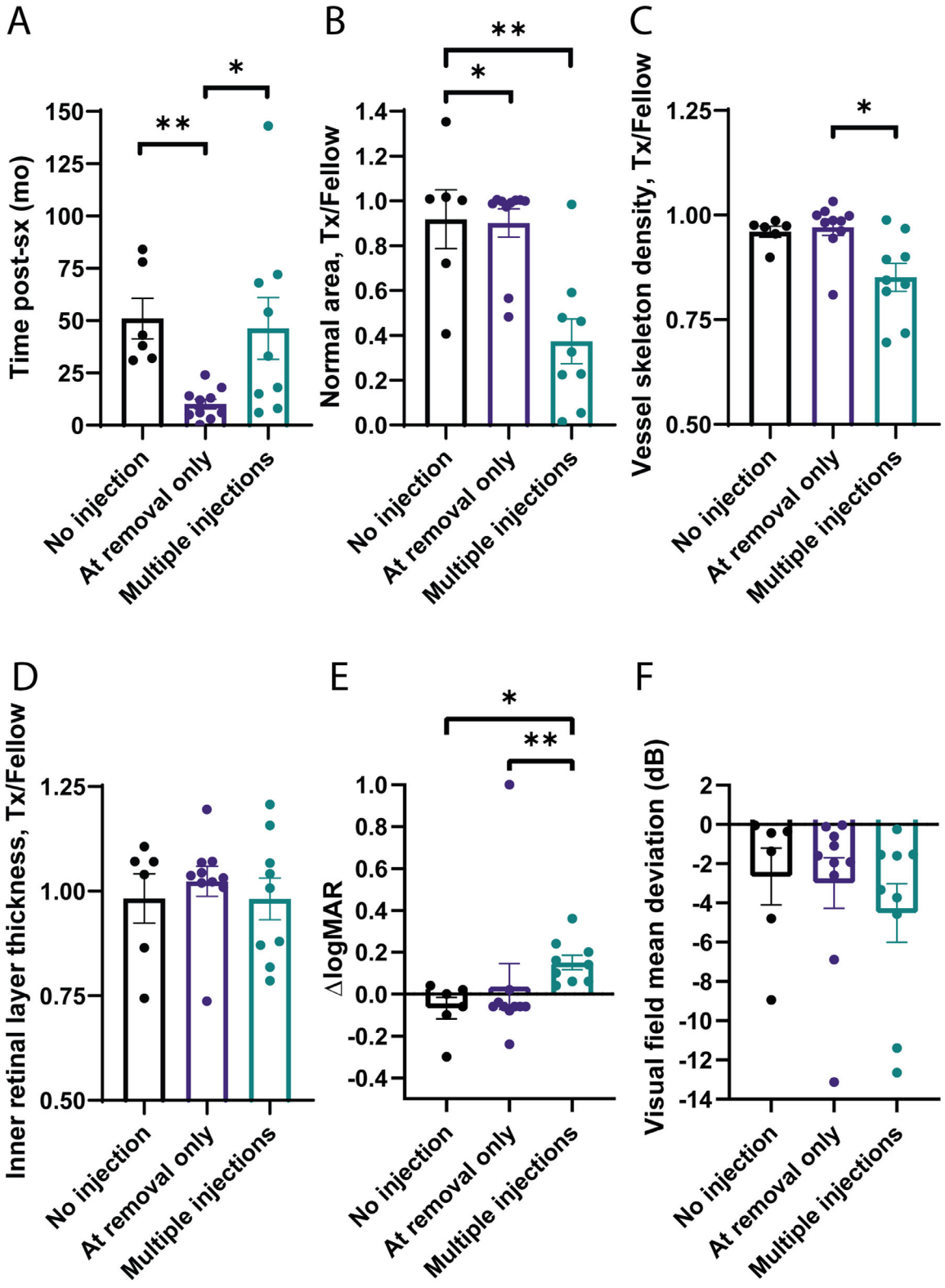

Figure 8. Effect of bevacizumab treatment on the appearance of visual field defect, retinal and microvascular pathology after ^{125}I-plaque brachytherapy. Patients without bevacizumab ($n = 6$), patients treated with one injection at plaque removal ($n = 10$) or treated with multiple prophylactic injections ($n = 9$) were compared for **(A)** time from plaque removal, **(B)** normal vascularity, **(C)** vessel skeleton density, **(D)** inner retinal layer thickness, **(E)** change in Snellen visual acuity by logMAR in the treated eye since time of tumor diagnosis; **(F)** mean deviation in decibels over the 10-2 visual field of the treated eye. All data are expressed as ratio in the treated (Tx) divided by the normal control (fellow) eye. *$P < 0.05$, **$P < 0.01$; Kruskal–Wallis ANOVA with Dunn's multiple comparisons test.

(Fig. 8A). Compared with the group that did not receive bevacizumab, significant differences were observed only for lacunarity, normal vascularity (Fig. 8B), avascularity, and change in logMAR visual acuity (Fig. 8E) when multiple injections were given. Patients who received one injection at removal showed better outcomes than those who received multiple injections. There was no difference between all groups for parafoveal density, inner retinal layer thickness (Fig. 8D), total retinal thickness, or neuronal function by visual field (Fig. 8F).

Discussion

In this study, we used different readouts to better understand the relationship between retinal microvasculopathy, retinal layer thinning as a surrogate of loss of neurons, and visual function in subjects treated with ^{125}I-plaque brachytherapy. There are several important findings. First, within the first 2 years after radiation treatment, the earliest phenotypical features of radiation retinopathy were related to microvascular pathology: leakage with fluid in the retinal layers by OCT, cotton wool spots, and small microaneurysms by digital fundus photography, as well as decreased vessel density by our novel OCT-A methods. These phenotypical features were associated with impaired retinal function as quantified by automated threshold perimetry of the central 10° of the macula. Moreover, at more than 2 years after brachytherapy, the microvasculopathy and neuron damage became more severe, with inner retinal layer thinning indicating a loss of retinal neurons. At later time points, all phenotypical features that could be quantified on a continuous scale highly correlated with one another.

Previous studies support repeat prophylactic administration of bevacizumab to slow FAZ enlargement, decrease retinal edema, and preserve visual acuity.[39–42] Here, patients who did not receive bevacizumab had significantly better visual acuity than those patients who did. There were no statistically significant differences in FAZ enlargement or retinal thickness across treatment groups. However, it is important to note that all patients who received only one injection at removal were seen within the first 2 years after plaque removal. For those groups with statistically significant differences, the group that received no bevacizumab had overall better outcomes, as did patients who received only one injection at plaque removal compared with those who received multiple injections. A potential explanation for these unexpected findings is that patients received multiple injections because of clinical evidence for retinopathy.

Although multiple studies have measured vascular abnormalities in both the irradiated and control eye of each patient,[15,43,44] previous studies reported the data from fellow eyes as a control group. Here, we paired each subject's treated eye with the fellow eye to account for any bilateral underlying abnormality not attributable to radiation retinopathy. Although interindividual differences in axial length would affect the absolute accuracy of some metrics reported here, for example, the size of the FAZ,[45,46] the use of intereye ratios to characterize each subject allows us to reliably compare different subjects. Furthermore, in our study subjects, there was no significant anisometropia. Moreover, we enrolled normal subjects to define a normal range of intereye asymmetry for all tests to provide the best estimate for deviation from normal anatomy in this cross-sectional study. Not surprisingly, because of our combined use of a control cohort and normalization to the fellow, untreated eye, changes in the FAZ area and parafoveal density, previously proposed as signs of early microvasculopathy,[13,14,47,48] were significantly less sensitive in detecting early abnormalities than our other readouts of capillary drop-out. We attribute the low sensitivity and specificity to a particularly wide range of intereye variability in FAZ area and parafoveal density in our normal cohort, and to our conservative definition of the normal range (within 3 SDs). These findings imply that measurements of FAZ area and parafoveal density may be useful when examined against baseline in a longitudinal study, but may not be sensitive enough as standalone metrics in a cross-sectional study or when no baseline measurement is available. In contrast, we found the measures of normal and hypovascular regions, as detected by our novel deep learning approaches[31] to be the best quantitative methods of detecting early vascular changes.

Whereas logMAR visual acuity only assesses central, foveal vision and is also influenced by nonretinal pathology, the 10-2 visual field protocol used here measures neuronal response to light stimuli across the same 6×6 mm^2 macular area where we measured vascularity and retinal thinning. Accordingly, the visual field mean deviation correlated with a change in inner retinal layer thickness ($P = 0.027$) as a measure of neuronal loss, in addition to most vascular measures. In contrast to visual acuity, visual field mean deviation also correlated with time from plaque removal ($P = 0.041$). These findings suggest a need for a measurement of retinal neuronal function, rather than foveal function alone, in a longitudinal study of radiation effects on the retina. We believe that using this method will allow for meaningful correlation of localized visual dysfunction with radiation dose, and vascular and neuronal pathology.

Limitations of this study include the need to exclude patients whose images were not of sufficient quality to accurately derive retinal layer thickness and vascularity. This factor likely represents an inherent problem in this study population, in whom the sequelae of radiation can induce cataracts, retinal scarring, and severe edema, and negatively impact image quality. A subanalysis of the excluded subjects revealed no significant demographic differences compared with the study population. This cross-sectional study provides first evidence for the concomitant development of microvascular and neuronal pathology in radiation retinopathy. The interpretation of retinal thinning over time can also be complicated by simultaneous thickening owing to intraretinal edema. Because this was a cross-sectional study, the time course of vascular and neuronal pathology could only be estimated by plotting the cumulative fraction of abnormal subjects with corresponding outcome measures at each time point.

A prospective longitudinal study, where images are acquired in an individual repeatedly over several years starting before brachytherapy, would be optimal to fully characterize the time course of vascular and neuronal pathology. This work would also reveal the role of prophylactic bevacizumab in the progression of radiation vasculopathy. Such data would provide more conclusive evidence as to whether microvascular injury causes retinopathy and precedes loss of function and neurons and would provide a basis for new treatment strategies.

Acknowledgments

The authors thank Connie Hinz and the UIHC Retina and Vitreous Clinic staff, especially Jan Full, Julie Nellis, and Joseph

Investigative Ophthalmology & Visual Science

Wetherell, for their support with clinical workflow, as well as Sriram Sugumaran for assistance with a preliminary analysis.

Supported by the American Heart Association (18IPA34170003 to IMG; 20PRE35110054 to MRT), the National Institutes of Health (R01 EY031544 to IMG, RHK, and MKG; T32 CA078586 to MRT), and the US Department of Veterans Affairs (I50RX003002 to RHK, MKG, and WD), and by a generous contribution from the Audre and Lavern Busse Family Foundation, and from the Al and Evelyn Mintzer Family (to RHK).

Disclosure: **M.R. Tamplin,** None; **W. Deng,** None; **M.K. Garvin,** None; **E.M. Binkley,** None; **D.E. Hyer,** None; **J.M. Buatti,** None; **J. Ledolter,** None; **H.C. Boldt,** None; **R.H. Kardon,** None; **I.M. Grumbach,** None

References

1. Tarlan B, Kiratli H. Uveal melanoma: current trends in diagnosis and management. *Turk J Ophthalmol.* 2016;46(3):123–137.
2. Aziz HA, Al Zahrani YA, Bena J, et al. Episcleral brachytherapy of uveal melanoma: role of intraoperative echographic confirmation. *Br J Ophthalmol.* 2017;101(6):747–751.
3. Harbour JW, Murray TG, Byrne SF, et al. Intraoperative echographic localization of iodine 125 episcleral radioactive plaques for posterior uveal melanoma. *Retina (Philadelphia, Pa).* 1996;16(2):129–134.
4. Aziz HA, Singh N, Bena J, Wilkinson A, Singh AD. Vision loss following episcleral brachytherapy for uveal melanoma: development of a vision prognostication tool. *JAMA Ophthalmol.* 2016;134(6):615–620.
5. Melia BM, Abramson DH, Albert DM, et al. Collaborative Ocular Melanoma Study (COMS) randomized trial of I-125 brachytherapy for medium choroidal melanoma. I. Visual acuity after 3 years COMS report no. 16. *Ophthalmology.* 2001;108(2):348–366.
6. Melia M, Moy CS, Reynolds SM, et al. Quality of life after iodine 125 brachytherapy vs enucleation for choroidal melanoma: 5-year results from the Collaborative Ocular Melanoma Study: COMS QOLS Report No. 3. *Arch Ophthalmol.* 2006;124(2):226–238.
7. Shields CL, Shields JA, Cater J, et al. Plaque radiotherapy for uveal melanoma: long-term visual outcome in 1106 consecutive patients. *Arch Ophthalmol.* 2000;118(9):1219–1228.
8. Heimann H, Coupland SE, Gochman R, Hellmich M, Foerster MH. Alterations in expression of mucin, tenascin-c and syndecan-1 in the conjunctiva following retinal surgery and plaque radiotherapy. *Graefes Arch Clin Exp Ophthalmol.* 2001;239(7):488–495.
9. Wen JC, Oliver SC, McCannel TA. Ocular complications following I-125 brachytherapy for choroidal melanoma. *Eye (Lond).* 2009;23(6):1254–1268.
10. Puusaari I, Heikkonen J, Kivela T. Ocular complications after iodine brachytherapy for large uveal melanomas. *Ophthalmology.* 2004;111(9):1768–1777.
11. Boldt HC, Melia BM, Liu JC, Reynolds SM, Group COMS. I-125 brachytherapy for choroidal melanoma photographic and angiographic abnormalities: the Collaborative Ocular Melanoma Study: COMS Report No. 30. *Ophthalmology.* 2009;116(1):106–115.e101.
12. Ramos MS, Echegaray JJ, Kuhn-Asif S, et al. Animal models of radiation retinopathy – from teletherapy to brachytherapy. *Exp Eye Res.* 2019;181:240–251.
13. Li Y, Say EA, Ferenczy S, Agni M, Shields CL. Altered parafoveal microvasculature in treatment-naive choroidal melanoma eyes detected by optical coherence tomography angiography. *Retina (Philadelphia, Pa).* 2017;37(1):32–40.
14. Say EA, Samara WA, Khoo CT, et al. Parafoveal capillary density after plaque radiotherapy for choroidal melanoma: analysis of eyes without radiation maculopathy. *Retina (Philadelphia, Pa).* 2016;36(9):1670–1678.
15. Skalet AH, Liu L, Binder C, et al. Longitudinal detection of radiation-induced peripapillary and macular retinal capillary ischemia using OCT angiography. *Ophthalmol Retina.* 2019;4(3):320–326.
16. Veverka KK, AbouChehade JE, Iezzi R, Pulido JS. Noninvasive grading of radiation retinopathy: the use of optical coherence tomography angiography. *Retina (Philadelphia, Pa).* 2015;35(11):2400–2410.
17. Schneider CA, Rasband WS, Eliceiri KW. NIH Image to ImageJ: 25 years of image analysis. *Nature Methods.* 2012;9(7):671–675.
18. Miura K, et al. 2014. *ImageJ Plugin CorrectBleach V2.0.2.* Zenodo, doi:10.5281/zenodo.30769.
19. Chen Q, Ma Q, Wu C, et al. Macular vascular fractal dimension in the deep capillary layer as an early indicator of microvascular loss for retinopathy in type 2 diabetic patients. *Invest Ophthalmol Vis Sci.* 2017;58(9):3785–3794.
20. Kim AY, Chu Z, Shahidzadeh A, Wang RK, Puliafito CA, Kashani AH. Quantifying microvascular density and morphology in diabetic retinopathy using spectral-domain optical coherence tomography angiography. *Invest Ophthalmol Vis Sci.* 2016;57(9):OCT362–OCT370.
21. Zhu T, Ma J, Li J, et al. Multifractal and lacunarity analyses of microvascular morphology in eyes with diabetic retinopathy: a projection artifact resolved optical coherence tomography angiography study. *Microcirculation.* 2019;26(3):e12519.
22. Sato Y, Nakajima S, Shiraga N, et al. Three-dimensional multi-scale line filter for segmentation and visualization of curvilinear structures in medical images. *Medical Image Analysis.* 1998;2(2):143–168.
23. Koulisis N, Kim AY, Chu Z, et al. Quantitative microvascular analysis of retinal venous occlusions by spectral domain optical coherence tomography angiography. *PloS One.* 2017;12(4):e0176404.
24. Bhardwaj S, Tsui E, Zahid S, et al. Fractal analysis of optical coherence tomography angiography in diabetic retinopathy with and without macular edema. *Invest Ophth Vis Sci.* 2017;58(8):30–34.
25. Mochi T, Anegondi N, Girish M, Jayadev C, Roy AS. Quantitative comparison between optical coherence tomography angiography and fundus fluorescein angiography images: effect of vessel enhancement. *Osli Retina.* 2018;49(11):E175–E181.
26. Huang F, Dashtbozorg B, Zhang J, et al. Reliability of using retinal vascular fractal dimension as a biomarker in the diabetic retinopathy detection. *J Ophthalmol.* 2016;2016:6259047.
27. Zahid S, Dolz-Marco R, Freund KB, et al. Fractal dimensional analysis of optical coherence tomography angiography in eyes with diabetic retinopathy. *Invest Ophthalmol Vis Sci.* 2016;57(11):4940–4947.
28. Matet A, Daruich A, Zografos L. Radiation maculopathy after proton beam therapy for uveal melanoma: optical coherence tomography angiography alterations influencing visual acuity. *Invest Ophthalmol Vis Sci.* 2017;58(10):3851–3861.
29. Backes A. A new approach to estimate lacunarity of texture images. *Pattern Recognition Letters.* 2013;34:1455–1461.
30. Karperien A. FracLac for ImageJ. 1999-2013, http://rsb.info.nih.gov/ij/plugins/fraclac/FLHelp/Introduction.htm.
31. Deng W, Tamplin MR, Grumbach IM, Kardon RH, Garvin MK. Region-based segmentation of capillary density in optical coherence tomography angiography. In: Fu H, Garvin M, MacGillivray T, Xu Y, Zheng Y , (eds). *Ophthalmic Medi-*

cal Image Analysis. OMIA 2019. Lecture Notes in Computer Science, vol. 11855. Cham: Springer; 2019.

32. Simonyan K, Zisserman A. Very deep convolutional networks for large-scale image recognition. *arXiv 14091556*. 2014.
33. Ronneberger O, Fischer P, Brox T. U-Net: convolutional networks for biomedical image segmentation. *arXiv 150504597*. 2015.
34. Antony BJ, Abramoff MD, Harper MM, et al. A combined machine-learning and graph-based framework for the segmentation of retinal surfaces in SD-OCT volumes. *Biomedical Optics Express*. 2013;4(12):2712–2728.
35. Garvin MK, Abramoff MD, Wu X, Russell SR, Burns TL, Sonka M. Automated 3-D intraretinal layer segmentation of macular spectral-domain optical coherence tomography images. *IEEE Trans Med Imaging*. 2009;28(9):1436–1447.
36. Rivard MJ, Coursey BM, DeWerd LA, et al. Update of AAPM Task Group No. 43 report: a revised AAPM protocol for brachytherapy dose calculations. *Medical Physics*. 2004;31(3):633–674.
37. Groenewald C, Konstantinidis L, Damato B. Effects of radiotherapy on uveal melanomas and adjacent tissues. *Eye (Lond)*. 2013;27(2):163–171.
38. Gunduz K, Shields CL, Shields JA, Cater J, Freire JE, Brady LW. Radiation retinopathy following plaque radiotherapy for posterior uveal melanoma. *Arch Ophthalmol*. 1999;117(5):609–614.
39. Daruich A, Matet A, Schalenbourg A, Zografos L. Intravitreal anti-vascular endothelial growth factor treatment at 2-month intervals reduces foveal avascular zone enlargement and vision loss in radiation maculopathy: a pilot study. *Retina (Philadelphia, Pa)*. 2019;39(8):1519–1526.
40. Finger PT, Chin K. Anti-vascular endothelial growth factor bevacizumab (Avastin) for radiation retinopathy. *Arch Ophthalmol*. 2007;125(6):751–756.
41. Shah SU, Shields CL, Bianciotto CG, et al. Intravitreal bevacizumab at 4-month intervals for prevention of macular edema after plaque radiotherapy of uveal melanoma. *Ophthalmology*. 2014;121(1):269–275.
42. Sagoo MS, Shields CL, Emrich J, Mashayekhi A, Komarnicky L, Shields JA. Plaque radiotherapy for juxtapapillary choroidal melanoma: treatment complications and visual outcomes in 650 consecutive cases. *JAMA Ophthalmol*. 2014;132(6):697–702.
43. Horgan N, Shields CL, Mashayekhi A, Teixeira LF, Materin MA, Shields JA. Early macular morphological changes following plaque radiotherapy for uveal melanoma. *Retina (Philadelphia, Pa)*. 2008;28(2):263–273.
44. Shields CL, Say EA, Samara WA, Khoo CT, Mashayekhi A, Shields JA. Optical coherence tomography angiography of the macula after plaque radiotherapy of choroidal melanoma: comparison of irradiated versus nonirradiated eyes in 65 patients. *Retina (Philadelphia, Pa)*. 2016;36(8):1493–1505.
45. Khan MH, Lam AKC, Armitage JA, Hanna L, To CH, Gentle A. Impact of axial eye size on retinal microvasculature density in the macular region. *Journal of Clinical Medicine*. 2020;9(8):2539.
46. Sampson DM, Gong P, An D, et al. Axial length variation impacts on superficial retinal vessel density and foveal avascular zone area measurements using optical coherence tomography angiography. *Invest Ophthalmol Vis Sci*. 2017;58(7):3065–3072.
47. Kinyoun JL. Long-term visual acuity results of treated and untreated radiation retinopathy (an AOS thesis). *Trans Am Ophthalmol Soc*. 2008;106:325–335.
48. Tan CS, Lim LW, Chow VS, et al. Optical coherence tomography angiography evaluation of the parafoveal vasculature and its relationship with ocular factors. *Invest Ophthalmol Vis Sci*. 2016;57(9):OCT224–OCT234.

Investigative Ophthalmology & Visual Science